Stochastic Environmental Research and Risk Assessment (2019) 33:2053–2069
https://doi.org/10.1007/s00477-019-01738-3

ORIGINAL PAPER

Wavelet analysis of precipitation extremes over India and teleconnections to climate indices

Maheswaran Rathinasamy[1,2] · Ankit Agarwal[2,3,4,7] · Bellie Sivakumar[5] · Norbert Marwan[2] · Jürgen Kurths[2,3,6]

Published online: 9 November 2019

Abstract

Precipitation patterns and extremes are significantly influenced by various climatic factors and large-scale atmospheric circulation patterns. This study uses wavelet coherence analysis to detect significant interannual and interdecadal oscillations in monthly precipitation extremes across India and their teleconnections to three prominent climate indices, namely, Niño 3.4, Pacific Decadal Oscillation, and Indian Ocean Dipole (IOD). Further, partial wavelet coherence analysis is used to estimate the standalone relationship between the climate indices and precipitation after removing the effect of interdependency. The wavelet analysis of monthly precipitation extremes at 30 different locations across India reveals that (a) interannual (2–8 years) and interdecadal (8–32 years) oscillations are statistically significant, and (b) the oscillations vary in both time and space. The results from the partial wavelet coherence analysis reveal that Niño 3.4 and IOD are the significant drivers of Indian precipitation at interannual and interdecadal scales. Intriguingly, the study also confirms that the strength of influence of large-scale atmospheric circulation patterns on Indian precipitation extremes varies with spatial physiography of the region.

Keywords Extreme precipitation · Teleconnection patterns · Wavelets · Partial wavelet coherence · India

Abbreviations

ENSO	El Niño-Southern Oscillation
IOD	Indian Ocean Dipole
PDO	Pacific Decadal Oscillation
SST	Sea surface temperature

1 Introduction

Climatic patterns of large-scale atmospheric circulation have been shown to significantly affect the variabilities and long-term persistence of precipitation. Investigation on the association of precipitation variabilities with low-frequency large-scale climatic fluctuations can further enhance our understanding of the physical dynamics of precipitation patterns (Agarwal et al. 2019; Araghi et al. 2017; Kim et al. 2008; Tan et al. 2016). For instance, our understanding of the regional teleconnections between low-frequency large-scale climatic fluctuations and the regional hydroclimatic variability has enhanced our ability to improve the prediction accuracy of monsoonal

Electronic supplementary material The online version of this article (https://doi.org/10.1007/s00477-019-01738-3) contains supplementary material, which is available to authorized users.

✉ Bellie Sivakumar
ankitfhy@iitr.ac.in; b.sivakumar@iitb.ac.in

[1] MVGR College of Engineering, Vizianagaram, India

[2] Research Domain Complexity Science, Potsdam Institute for Climate Impact Research, Telegrafenberg, 14412 Potsdam, Germany

[3] Institute of Earth and Environmental Science, University of Potsdam, Potsdam, Germany

[4] GFZ German Research Centre for Geosciences, Section 4.4: Hydrology, Telegrafenberg, 14412 Potsdam, Germany

[5] Department of Civil Engineering, Indian Institute of Technology Bombay, Powai, Mumbai 400 076, India

[6] Institute of Physics, Humboldt Universität zu Berlin, 12489 Berlin, Germany

[7] Department of Hydrology, Indian Institute of Technology Roorkee, Roorkee 247667, Uttrakhand, India

precipitation, which will be useful for efficient water resource management (Khedun et al. 2014; Konapala et al. 2018; Wang et al. 2014; Yoon et al. 2013). Similarly, an advanced understanding of the teleconnection of climatic patterns with hydrological processes, such as streamflow and soil moisture, can be used for investigating the occurrence of extreme hydrological events (Niu 2013; Niu et al. 2014).

The Indian climate is significantly influenced by several natural large-scale climatic patterns, such as the El Niño-Southern Oscillation (ENSO), the Indian Ocean Dipole (IOD), the Pacific Decadal Oscillation (PDO) as well as other teleconnection patterns, as reported by many studies (Azad and Rajeevan 2016; Krishnamurthy and Goswami 2000; Krishnan and Sugi 2003; Li and Chen 2014; Mokhov et al. 2012). Such studies, in particular, have examined the teleconnections between large-scale climatic patterns and Indian precipitation and explained the inter-dependency of the climate indices. For instance, Kumar (1999) analysed a 140-year historical precipitation record and observed an inverse relationship between ENSO and the Indian summer monsoon precipitation (ISMR), i.e. weak monsoon arising from warm ENSO events. Krishnamurthy and Goswami (2000), using reanalysis product, explained that the physical link through which ENSO is related to decreased monsoon precipitation exists on both interannual and interdecadal timescales. Ashok et al. (2004) reported that ENSO and IOD had complementarily affected the ISMR during the previous four decades; whenever the ENSO–ISMR correlation was low (high), the IOD–ISMR correlation was high (low). In a later study, Ashok et al. (2007) showed that IOD significantly influences the Indian summer monsoon precipitation and simultaneously reduces the impact of ENSO on the Indian summer precipitation, whenever these events co-occur in the same phase. Bhatla et al. (2016) showed that the effect of PDO on the Indian precipitation has significantly strengthened in the more recent years as compared to that in the earlier years. The study by Azad and Rajeevan (2016) revealed a statistically significant inverse relationship between the ENSO events and the Indian summer monsoon precipitation.

It is important to note that most of these studies have been based on the analysis of monthly precipitation or monsoonal precipitation. Although such studies are useful for precipitation forecasting and water management at monthly, seasonal, and longer scales, they are often inappropriate and insufficient for studying precipitation extremes. To the best of our knowledge, studies on the teleconnections between large-scale climatic patterns and extreme precipitation in India are almost non-existent, despite the fact that such studies have been conducted for other regions; for instance, the study by Cazes-Boezio et al. (2003) identified the seasonal dependence of ENSO teleconnections over South America and relationships with precipitation in Uruguay. Grimm (2011) and Grimm and Tedeschi (2009) re-examined the teleconnections between extreme precipitation and ENSO in South America and suggested that the ENSO-related changes in extremes are much more extensive than the corresponding changes in seasonal rainfall because the highest sensitivity to ENSO seems to be in the extreme range of daily precipitation. Following these, Niu (2013) and Niu et al. (2014) investigated the teleconnection patterns of precipitation (and soil moisture) in the Pearl River basin in South China with IOD and ENSO as the indices. Shi et al. (2016) investigated the temporal trends and spatial distributions of precipitation as well as related meteorological variables, analyzed the relationship between precipitation and elevation over the Three-River Headwaters Region in China. Recently, Boers et al. (2019), Agarwal et al. (2019), Kurths et al. (2019) and Ekhtiari et al. (2019) have revealed the global pattern of extreme rainfall teleconnections by analysing the atmospheric conditions that lead to these teleconnections. The study by Boers et al. (2019) further showed Rossby waves as the physical mechanism underlying these global teleconnection patterns and emphasizes their crucial role in dynamical tropical–extratropical couplings.

In examining the teleconnections, studies have generally used simple regression analysis, empirical orthogonal function analysis, principal component analysis, wavelet analysis, and correlation measure (e.g. Pearson's correlation coefficient). For instance, Ihara et al. (2008) used multiple linear regression analysis to identify the possible relation between the annual maximum precipitation and different climatic indices. Curtis et al. (2007) and Alexander et al. (2009) used the statistically significant Pearson correlation between precipitation extremes and large-scale climate anomalies. Cioffi et al. (2017), Duan et al. (2015) and Gan et al. (2007) have shown the advantage of wavelet analysis to study the correlation of extreme precipitation with climate indices over Canada, Europe, and Japan, respectively. Other studies that have used wavelets include those by Zhao et al. (2014) and Tan et al. (2016), which have employed wavelet coherence analysis (WCA) to study the possible effects of climate indices on extreme precipitation.

While the above studies have yielded encouraging outcomes on the relationship between large-scale climate patterns and precipitation, they have not considered the interdependency while investigating the teleconnection patterns. However, some of the large-scale circulation patterns are essentially interdependent (Gan et al. 2007; Lorenzo et al. 2008). For example, precipitation (P) might be influenced by two variables X_1 and X_2, which themselves may be correlated. In this scenario, analysis of the relationship between P and X_1 using the wavelet coherence

analysis inherently considers also the effect of X_2. This might result in an erroneous interpretation of the actual relationship between P and X_1. Therefore, it is important to study the standalone effect of every climate index on precipitation separately, for a more informed and reliable means for developing prediction models. This provides the motivation for the present study.

The overall objectives of the present study are twofold: (1) to detect significant interannual and interdecadal oscillations in the extreme precipitation (estimated in terms of the monthly maximum daily data) in India and their teleconnections with large-scale anomalies over different climatic regions; and (2) to estimate the standalone relationship between each climate index and the extreme precipitation in India. To achieve these, wavelet analysis and partial wavelet coherence analysis are performed on the daily precipitation dataset in India. Gridded daily precipitation data over the period 1901–2013, provided by the India Meteorological Department (IMD), are analysed.

The rest of this paper is organized as follows. Section 2 presents details of the Indian precipitation data and the large-scale climate indices. Section 3 describes the mathematical details of wavelet analysis and its variants used in this study. Section 4 presents the results of the application of the wavelet methodology to the Indian daily precipitation data, and a discussion of the results is made in Sect. 5. The conclusions are briefed in Sect. 6.

2 Study area and data

The Indian precipitation patterns have been extensively studied using the gridded daily precipitation data set at 0.25° × 0.25° spatial resolution (Pai et al. 2015), released by the IMD. The data are available for the period 1901–2013. Details about these data can be obtained from http://imd.gov.in (homepage/Rainfall information). In the present study, we use the precipitation data over this period for investigating the influence of teleconnections on extreme precipitation (Agarwal 2019).

At the spatial resolution of 0.25° × 0.25°, there is a total of 4631 grid points for the Indian subcontinent. As different parts of India have different climatic conditions and precipitation patterns, it would be more appropriate to study the teleconnections with respect to different regions. Therefore, we divide the entire country (Fig. 1) into a number of homogeneous regions, and examine the teleconnections for each of the identified homogeneous regions. For identification of homogeneous regions in the Indian subcontinent, we use complex networks-based community detection algorithm, following the methods proposed by Rheinwalt et al. (2015) and Agarwal et al. (2018); for details about the complex networks concepts, including community structure methods, and the formation of the homogeneous regions, the readers are directed to Agarwal et al. (2018). Figure 1 shows seven homogeneous regions identified, as follows: Peninsular (Community 1); West central (Community 2); Central north east and the Western Ghats (Community 3); North east (Community 4); North west (Community 5); Coastal north west (Community 6); and Hilly region (Community 7).

To analyse adequately the temporal variability in extreme precipitation in India and to investigate the spatial variability of the teleconnections, we consider daily precipitation data from a total of 30 grid points falling on important cities spread across the country (as shown in Fig. 1), and fairly evenly distributed in the seven identified homogeneous regions. For each of these 30 grid locations, the monthly maximum daily precipitation time series is extracted from the daily data. The precipitation anomalies are obtained by subtracting the monthly mean extreme precipitation from the monthly maximum time series and then dividing it by the standard deviation of precipitation in that month.

In this study, three monthly climate indices of large-scale circulation patterns are considered: ENSO (represented by Niño 3.4), PDO, and IOD. We select only these three prominent climatic indices, as they have been shown to have a significant relationship with the Indian monsoon (However, the same approach detailed in the following sections can also be used when other pertinent indices are considered, as appropriate). The data for these three climate indices are obtained from the National Oceanographic and Atmospheric Administration (NOAA) website: http://www.esrl.noaa.gov/psd/data/climateindices. A brief summary of the three climate indices is presented here.

(a) The Niño 3.4 index is one of the several indices used to measure the ENSO effect. It is estimated as the average SST anomaly in the region bounded by 5° N to 5° S, from 170° W to 120° W. Maity and Nagesh Kumar (2006) and several others have shown some notable influence of Niño 3.4 on the Indian monsoon.

(b) The PDO is an ocean-atmospheric climate index, which recurs over the mid-latitude Pacific. Krishnamurthy and Krishnamurthy (2016) reported the Indian monsoon precipitation decadal oscillations to be associated with the decadal variability of the PDO.

(c) The Indian Ocean Dipole (IOD) index is represented by the anomalous SST gradient between the western equatorial Indian Ocean (50° E–70° E and 10° S–10° N) and the south eastern equatorial Indian Ocean (90° E–110° E and 10° S–0° N). Several studies (Ashok et al. 2004; Behera and Ratnam 2018) have shown that IOD plays a key role in the climate of the Indian subcontinent.

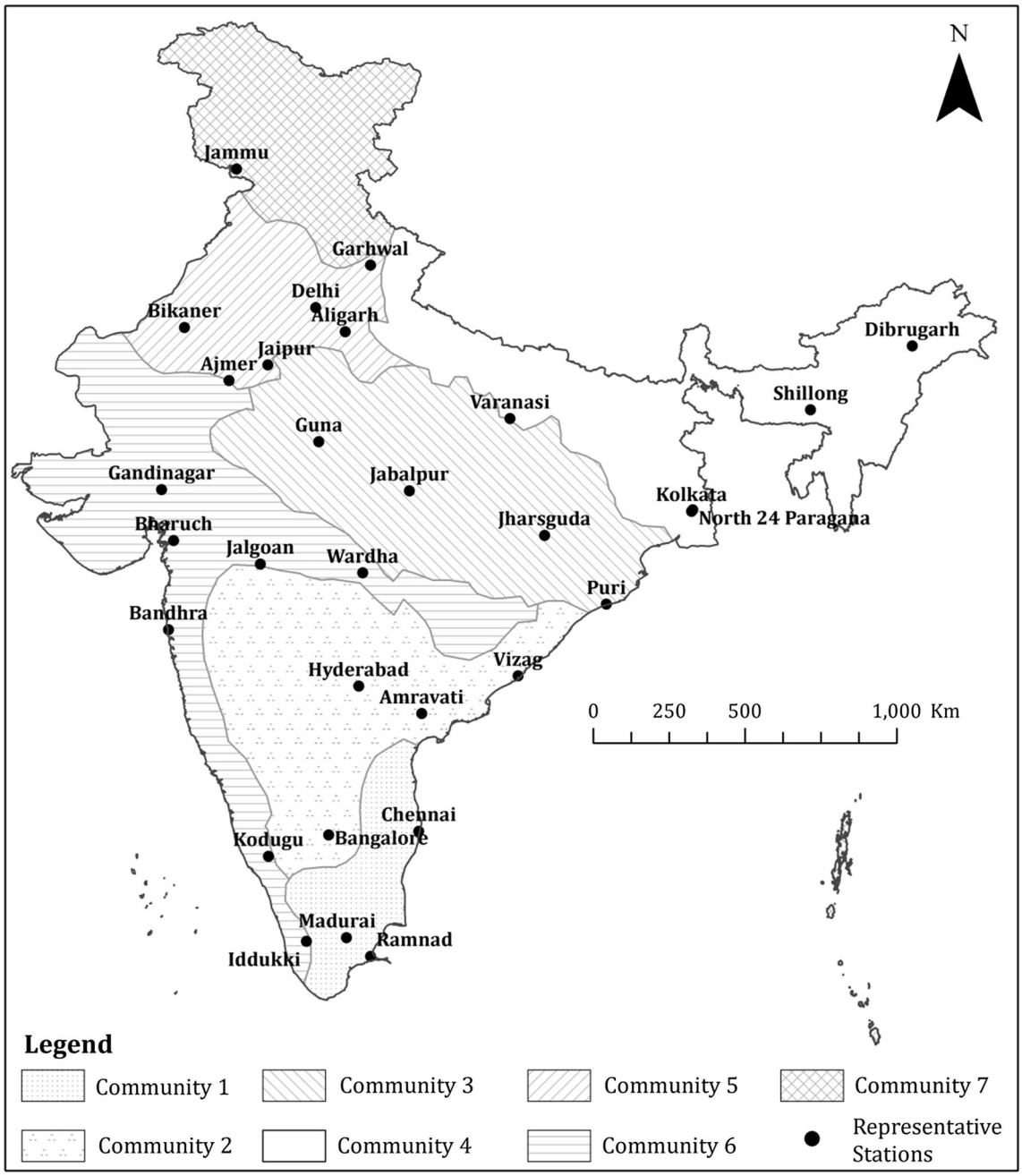

Fig. 1 Map of India showing seven homogeneous climatic regions/precipitation patterns and geographic locations of 30 stations considered in the present study

These climate indices (and two others—NAO and AMO) are significantly interdependent on each other (at 95% confidence levels) for the different seasons in India (Table 1). For instance, during the southwest monsoon season (June, July, August, and September), the relationship between Niño 3.4 and PDO is found to be statistically significant. Furthermore, Niño 3.4 and IOD have significant correlation for some seasons.

3 Methodology

In the present study, we use the continuous wavelet transform (CWT) to extract the dominant oscillations of the Indian extreme precipitation and the wavelet coherence analysis (WCA) to study the teleconnection relationship of precipitation with the climate indices. We also employ the partial wavelet coherence analysis (PWCA) to study the standalone relationship between a climate index series and

Table 1 Pearson correlation coefficients between different climate indices for different seasons in India

Months		NINO3.4	PDO	IOD	NAO	AMO
	NINO3.4	1				
	PDO	**0.39203**	1			
DJF	**IOD**	**0.127694**	0.006052	1		
	NAO	− 0.0014	− 0.001	− 0.0053	1	
	AMO	0.045	− 0.025	− 0.005	− 0.116	1
	NINO3.4	1				
	PDO	**0.382566**	1			
MAM	**IOD**	0.129083	0.072002	1		
	NAO	0.025	− 0.090	− 0.049	1	
	AMO	0.266	− 0.121	0.169	− 0.100	1
	NINO3.4	1				
JJAS	**PDO**	**0.500945**	1			
	IOD	**0.15391**	0.0693	1		
	NAO	− 0.0148	− 0.048	− 0.054	1	
	AMO	0.002	0.028	0.077	− 0.125	1
	NINO3.4	1				
	PDO	**0.375404**	1			
ON	**IOD**	**0.181336**	0.03559	1		
	NAO	0.072	0.021	0.056	1	
	AMO	− 0.081	0.040	− 0.0127	− 0.091	1

Bold indicates the correlation values are significantly different from zero at 95% confidence levels

the extreme precipitation time series. A detailed description of the wavelet analysis procedure is presented below.

3.1 Continuous wavelet transform (CWT)

Wavelet analysis is a multi-resolution analysis used to obtain time–frequency representations of a continuous signal. Wavelet analysis transforms a signal into scaled and translated versions of an original (mother) wavelet, instead of decomposing a signal into constituent harmonic functions as in Fourier analysis. The wavelet transform is defined as (Daubechies 1992)

$$W(a,\tau) = \frac{1}{\sqrt{|a|}} \int_{-\infty}^{\infty} f(t)\psi\left(\frac{t-\tau}{a}\right)dt \tag{1}$$

where ψ represents the family of functions called wavelets, t represents the instant of time, a and τ are the scale and location parameters. The above defined transform is the continuous wavelet transform (CWT), because the scale and time parameters, a and τ, assume continuous values (Torrence and Compo 1998). The CWT provides a redundant representation of the signal $f(t)$, as the original signal can be reconstructed with the minimum of $W(a,\tau)$ values. The reconstruction of the signal $f(t)$ can be obtained using (Daubechies 1992)

$$f(t) = \frac{1}{C_\psi} \int_{-\infty}^{\infty} \int_{0}^{\infty} a^{-2} W(a,\tau)\psi_{a,\tau}(t)dad\tau \tag{2}$$

where C_ψ is a constant and depends on the choice of the wavelet ψ. Clearly, Eq. (2) suggests that the function $f(t)$ may be seen as a superposition of signals at different scales and obtained by varying the scale parameter 'a'.

Further, the energy of the signal $f(t)$ can be represented scale-wise as (Daubechies 1992)

$$\int_{-\infty}^{\infty} f^2(t)dt = \frac{1}{C_\psi} \int_{0}^{\infty} \left[\int_{-\infty}^{\infty} |W(a,\tau)|^2 d\tau \right] \frac{da}{a^2} \tag{3}$$

Although the left-hand side of Eq. (3) is called the 'energy' of the signal $f(t)$, it is not really energy in the physical sense, unless $f(t)$ has the proper units. We can, thus, interpret $[W(a,\tau)]^2 d\tau$ as being proportional to an energy density function that decomposes the energy in $f(t)$ across different scales and times. Flandrin (1988) denoted the function $|W(a,\tau)|^2$ as a 'scalogram.' For two different functions $f(t)$ and $g(t)$, the product of $W_f(a,\tau)$ and $W_g(a,\tau)$ may be called a 'cross-wavelet transform' (Lakhanpal et al. 2017), which is described next.

3.2 Cross-wavelet transform (XWT)

While, in general, wavelet transform provides an unfolding of the characteristics of a process in the scale-space plane, a cross-wavelet transform (XWT), on the other hand, provides a similar unfolding of possible interactions of two processes. Therefore, this measure can reveal the structure of a particular process or the interactions between different processes at different scales. The cross-wavelet transform identifies the cross-wavelet power of two time series. For two given discrete time series, X (n = 1, 2, …, N) and Y (n =1, 2, …, N), the cross-wavelet spectrum, W^{XY}, is calculated as

$$W^{XY}(a) = W^{X}(a) \times W^{Y*}(a) \tag{4}$$

where $W^{X}(a)$ is the CWT of time series X and $W^{Y*}(a)$ is the complex conjugate of $W^{X}(a)$, the CWT of time series Y.

3.3 Wavelet coherence (WC)

The cross wavelet spectrum reveals the areas with high common power. However, it can potentially lead to misleading results, as it is just the product of two non-normalized wavelet spectra (Maraun and Kurths 2004). This can be overcome by using wavelet coherence, where the cross spectrum is normalized with respect to the wavelet energy of X and Y. The wavelet coherence between two time series X and Y is given by:

$$R(X,Y) = \frac{\varsigma[\mathrm{W}(\mathrm{X},\mathrm{Y})]}{\sqrt{\varsigma[W(X)]\varsigma[W(Y)]}} \qquad R^2(X,Y) = R(X,Y)\cdot R(X,Y)^*; \tag{5}$$

where $R(X,Y)$ is the measure of the wavelet coherence between Y and X; R^2 (X, Y) is the measure of the squared wavelet coherence between Y and X; W (X, Y) denotes the corresponding cross-wavelet transform; $W(.)$ denotes the wavelet transform; and ς denotes a smoothing operator that can be used to balance between the desired time–frequency resolution and statistical significance. The wavelet coherence ranges from 0 to 1 and measures the cross-correlation of two time series as a function of frequency (Torrence and Compo 1998), i.e. local correlation between the time series in time–frequency space. It can be interpreted as a decomposition of correlation coefficient at a different scale (Agarwal et al. 2016); the closer the value to 1, the more the correlation between the two series.

3.4 Partial wavelet coherence analysis (PWCA)

Partial wavelet coherence analysis (PWCA) is a technique similar to the partial correlation analysis that helps to find the resulting wavelet coherence between two time series X and Y after eliminating the influence of the time series Z. Mihanović et al. (2009) extended the concept from simple linear correlation and suggested that the square of PWC (after the removal of the effect of Z) can be defined by an equation similar to the square of partial correlation, which is like the simple wavelet coherence, ranging from 0 to 1, and is given by

$$RP^2(X,Y|Z) = \frac{|R(X,Y) - R(X,Z).R(X,Y)^*|^2}{[1-R(X,Z)]^2[1-R(Y,Z)]^2} \tag{6}$$

where R (.,.) denotes the wavelet coherence between the two variables and $RP^2(X, Y|Z)$ is the square of the partial wavelet coherence between X and Z when the influence of Y is excluded. Its proximity to zero at a certain time–frequency point indicates that the series Z does not add significant information to X, i.e. the information that is not already incorporated from Y at that point. If the square of the partial wavelet coherence is high for Y and not for Z, this would imply that important covariance exists between Y and X during that time interval at a designated wavelet scale (period) and, moreover, that X is dominantly influenced by Y and not by Z. If both $RP^2(X, Y|Z)$ and $RP^2(X, Z|Y)$ still have significant bands, both Y and Z have a significant influence on X.

In the present study, we adopt the Grinsted Toolbox for wavelet coherence analysis and the toolbox provided by Ng and Chan (2012) for PWCA. In all the analyses, we use the 95% significance levels.

4 Results

4.1 Wavelet analysis

To understand the variability of extreme precipitation with reference to time, Continuous Wavelet Transform (CWT) analysis is performed using the 'Morlet' wavelet. The Morlet wavelet is chosen for analysis because it is a widely used complex wavelet and has a better time–frequency localization than other real wavelets (Addison 2005). However, it is also relevant to note that the choice of the wavelet does not make much difference in this kind of multiscale coherence analysis (Foufoula-Georgiou and Kumar 1994; Gan et al. 2007).

Figure 2 presents the wavelet coefficients obtained from the CWT for the extreme precipitation at seven selected grids/cities (one grid from each homogeneous region): Chennai, Bangalore, Varanasi, Dibrugarh, Delhi, Gandhinagar, and Jammu; see Fig. S1 for all the 30 grids. The thick contour lines enclose regions of statistically significant wavelet power in the time–frequency space at a 5%

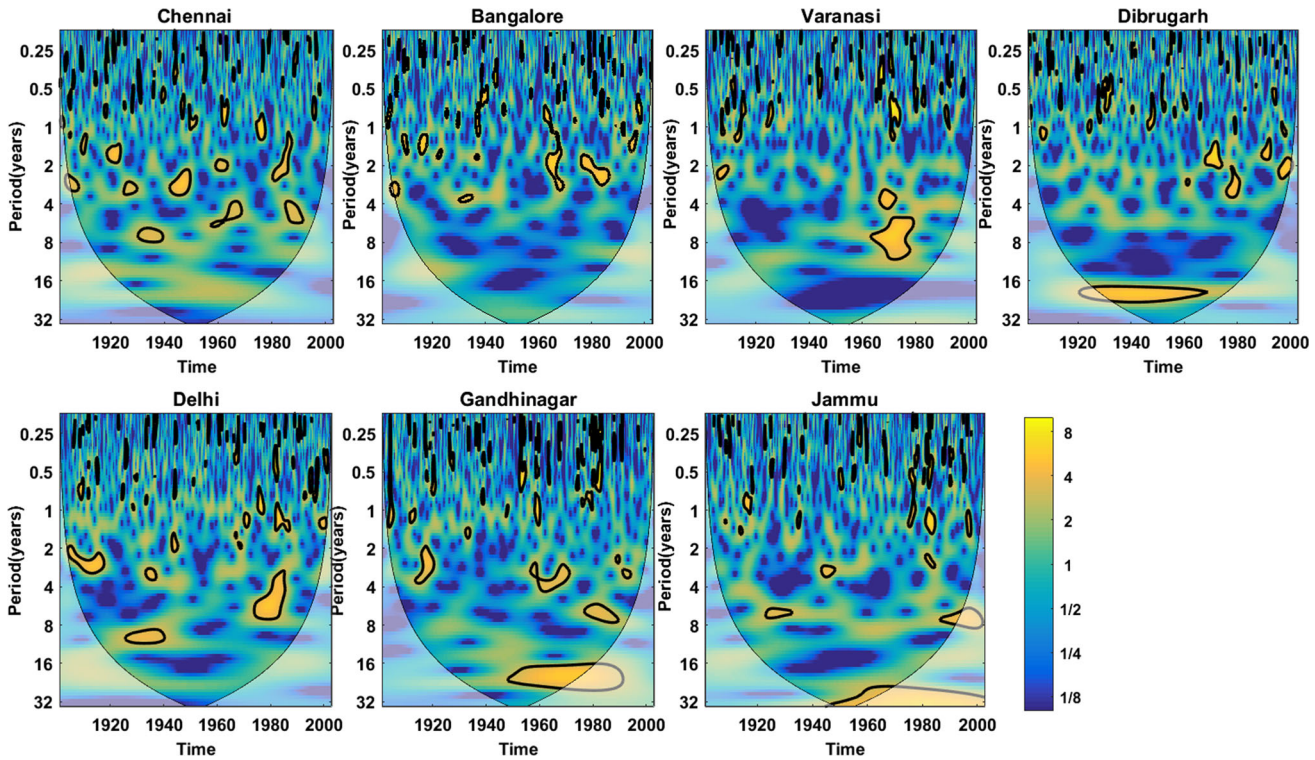

Fig. 2 Wavelet power spectra of extreme precipitation time series from seven locations (one from each of the seven homogeneous regions) with the 95% confidence level. The thick black contours depict the 95% confidence level of local power relative to a red noise background

significance level of a red noise process (Grinsted et al. 2004). Significant interannual oscillations (4–8 years) occurred in the 1900s to 1980s at Varanasi (North India). Interdecadal oscillations (> 8 years) were active from 1920s to 1970s in Dibrugarh (Northeast), from 1950s to 2000s in Jammu (far North) and from 1950s to 1990s in Gandhinagar (West). In the case of Chennai (Southeast), Delhi (North) and Bangalore (South central), it can be observed that there are some intermittent high power regions at 2–4 years and 4–8 years scales. These figures clearly show the spatial variability of the precipitation extremes and the corresponding dominant oscillations.

Figure 3 presents the wavelet coefficients from the CWT for the three climate indices (Niño 3.4, PDO, and IOD) to understand the dominant oscillations that are active in each index. It can be observed that the Niño3.4 is characterised by 2–4 years and 4–8 years oscillations. However, these oscillations are not stationary with respect to time. Even though there is evidence of 8–16 years oscillations, it is not statistically significant. The CWT of

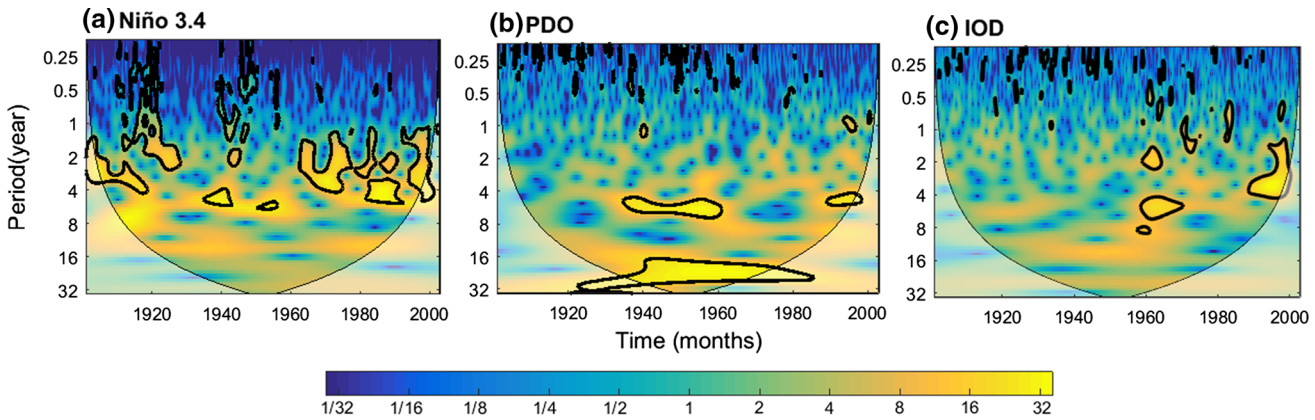

Fig. 3 Continuous wavelet spectrum of the climate indices, **a** Niño 3.4; **b** PDO; **c** IOD with the 95% confidence level. The thick black contours depict the 95% confidence level of local power relative to a red noise background

the PDO reveals that it is generally characterised by significant large-scale decadal oscillations in the order of 16–32 years. We can also observe a short-term oscillation at 4–8 years active only for the period from 1935 to 1960. In the case of the IOD, there is evidence of intermittent significant oscillations at 4–8 years from 1960 to 1970 and at 2–4 years from 1990 to 2000.

4.2 Wavelet coherence analysis (WCA)

The wavelet coherence analysis (WCA) is used to statistically estimate the linkages between extreme precipitation and the selected climate indices. Figures 4, 5, and 6 show the results for the above seven grids/cities for ENSO, PDO, and IOD, respectively (see Figs. S2–S4 for all the 30 grids). The black contours in these figures represent periods of statistically significant coherence of a thick red noise process at 5% significance levels (Grinsted et al. 2004). It is important to note that significant coherence between two signals do not necessarily mean that the powers of the two signals are also statistically significant, but rather that it might be showing significant coherence.

A significant coherence between Niño 3.4 and precipitation anomalies at the scale of 2–4 years, 4–8 years and 8–16 years is present (Fig. 4). However, interannual coherence is of short duration and transient in nature. This may be attributed to the fact that Niño 3.4 episodes are mostly short-lived. For example, in the case of Chennai, strong coherence is observed during the periods 1953–1956, 1970–1971, 1982–1990, and 1998–2000. It is also observed that these time periods were matching with the La Niña incident years. From these wavelet coherence plots, we can locate the time periods of high coherence, weakening coupling or even the absence of significant coupling between Niño 3.4 and precipitation. Following a similar analysis for the other stations shown in Fig. 4, it can be observed that the coherence between Niño 3.4 and precipitation has become stronger in the recent decades (as shown by the yellow areas after 1960) in most parts of the country except for the northern parts (e.g. Delhi). The wavelet coherence plots for different regions differ significantly (Fig. S2). Precipitation at some stations, such as Madurai, Bangalore, Varanasi, Delhi, and Jaipur, does not have significant coherence with Niño 3.4 at 16–32 years scale, whereas other stations, such as Chennai, Kolkata, Gandhinagar, Bandhra, and Shillong, have significant Niño 3.4 influence at that larger scale.

Comparing PDO with the extreme precipitation at the seven locations with the wavelet coherence reveals a consistent significant coherence at larger scales of the order of 8–16 years, indicating a high correlation between extreme precipitation and PDO at these scales (Fig. 5; see Fig. S3

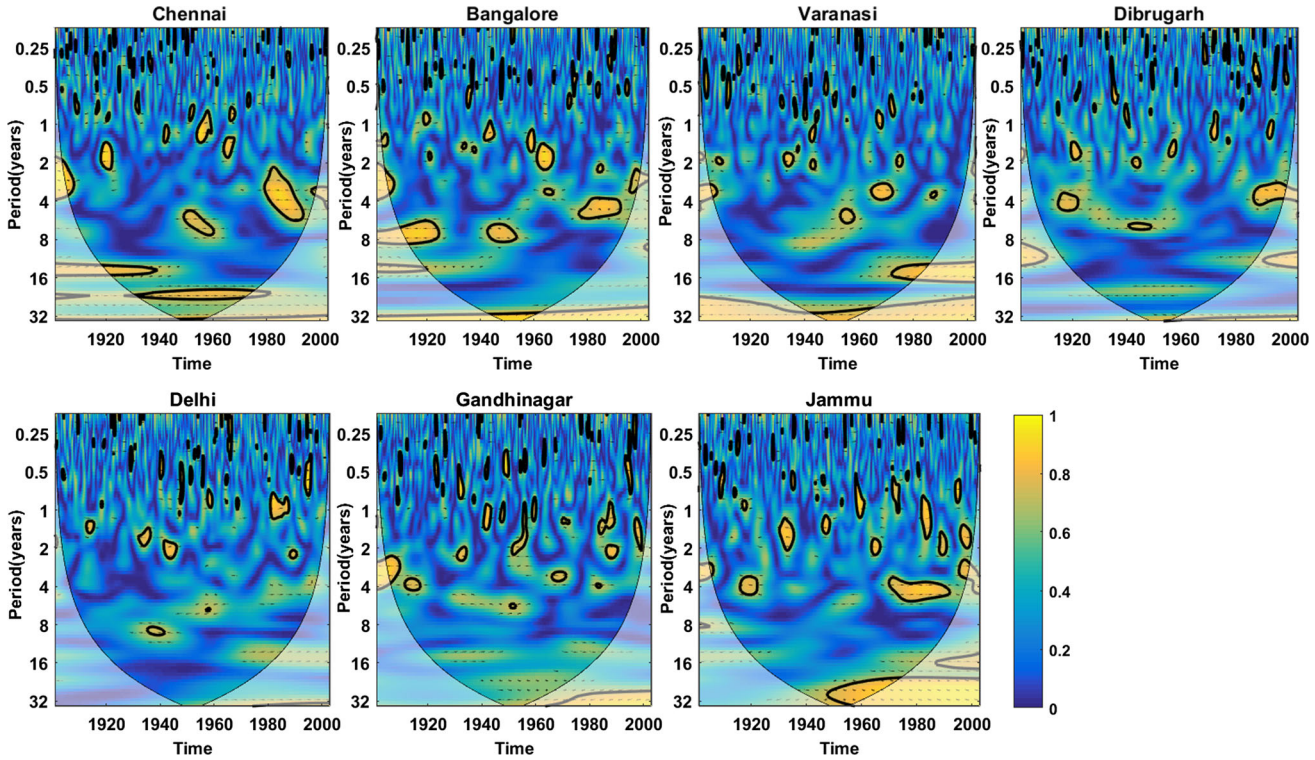

Fig. 4 Wavelet coherence spectra between extreme precipitation from seven locations (one from each of the seven homogeneous regions) and Niño 3.4. The thick contour lines enclose periods with statistically significant coherence with reference to a red noise process at 5% significance level

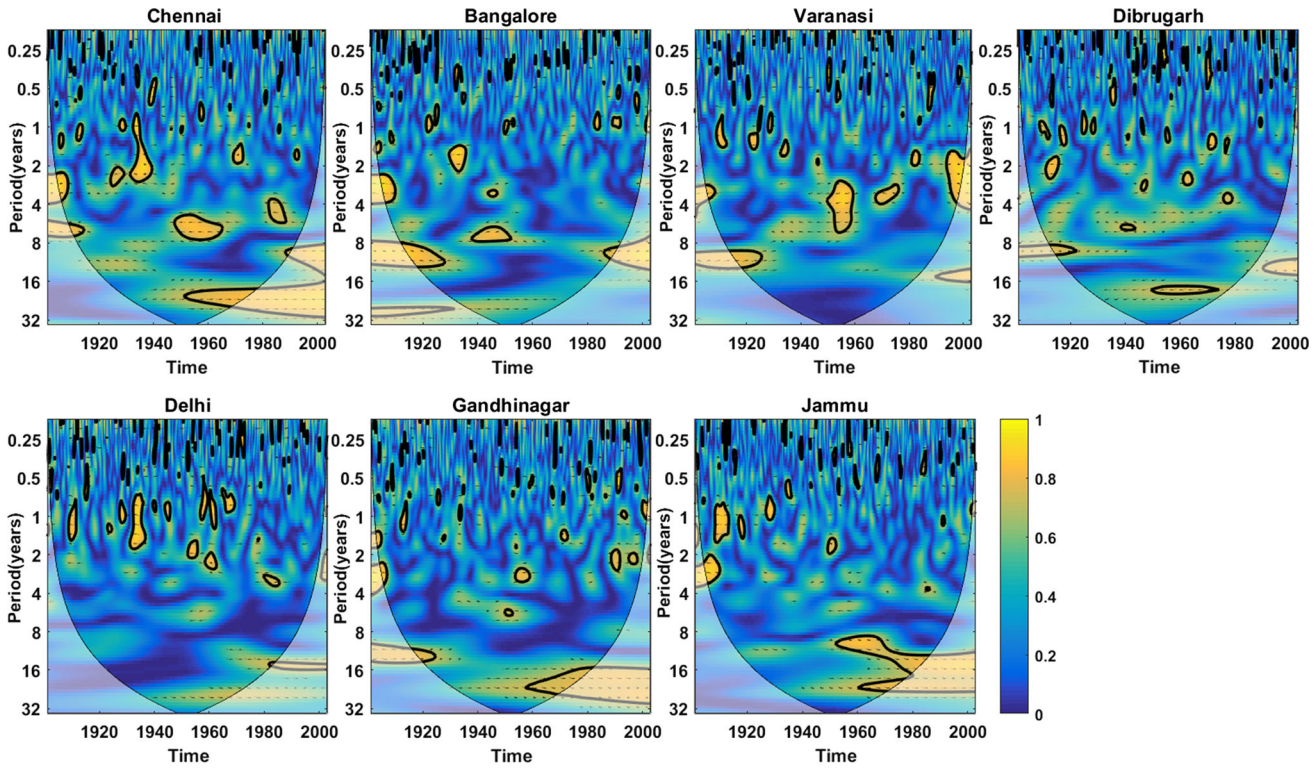

Fig. 5 Same as Fig. 4, but with PDO as the climate index

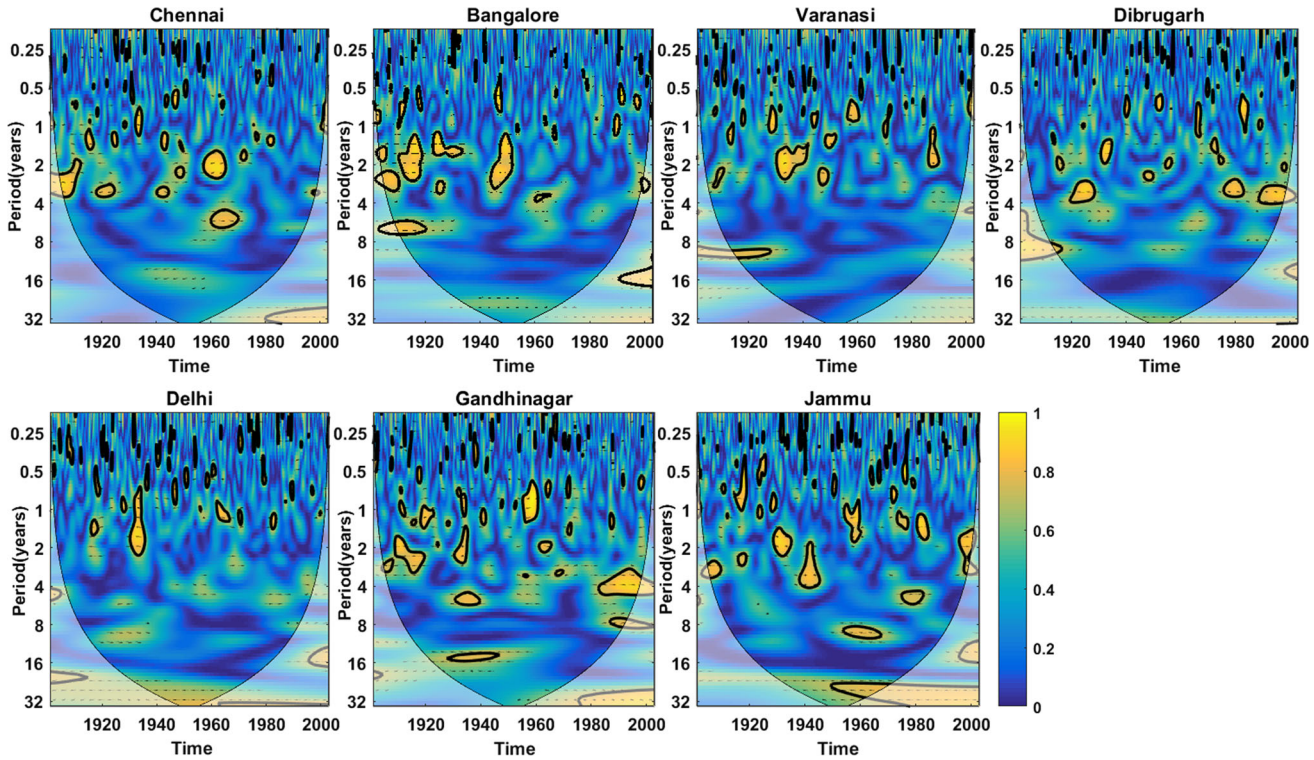

Fig. 6 Same as Fig. 4, but with IOD as the climate index

for all 30 locations). Apart from this consistent long-term feature, there are only a few intermittent high-power regions.

The WCA between extreme precipitation and IOD for the seven locations indicates a significant coherence between the extreme precipitation and IOD for the majority of the locations at interdecadal scales of order of 16–32 years (Fig. 6; see Fig. S4 for all 30 locations). At some locations, such as Chennai, Bengaluru, Gandhinagar, and Jammu, there is a significant but intermittent high coherence at 2–4 and 4–8 years. In this case, also, the spatial variability of the wavelet coherence between the extreme precipitation and IOD is high. For example, there is no coherency between extreme precipitation and IOD at Delhi, whereas there is a statistically significant coherence between the two in, for example, Jammu, Wardha, and Aligarh.

The above results reveal the spatial and temporal variability in the relationship between extreme precipitation in India and the three climate indices. The results from the wavelet coherence analysis suggest that extreme precipitation is related to all the three climate indices (Niño 3.4, PDO, and IOD), but at different scales and at varying degrees. However, it should be noted that there is a significant level of interdependence among the climate indices, as shown in Table 1. Therefore, for a still better understanding of the dynamics of the influence of the climate indices on extreme precipitation, it is also necessary to understand the standalone effect of the indices on the extreme precipitation. To this end, we perform the Partial Wavelet Coherence Analysis (PWCA), and the results are presented next.

4.3 Partial wavelet coherence analysis (PWCA)

Several past studies have established relationships among the climate indices, especially the influence of ENSO. For instance, Hanley et al. (2003) showed the dependence of PDO on ENSO events (Niño 3.4), and Ashok et al. (2004) discussed the relationship between IOD and ENSO events (Niño 3.4 or SOI). These studies indicate that ENSO events (Niño 3.4 or SOI) play an influencing role in controlling the other climate indices. From this perspective, we now remove the effect of Niño 3.4 and examine only the coherence between the standardized extreme precipitation and each of the other two climate indices (PDO and IOD). This would also help in understanding the standalone effect of PDO and IOD on Indian extreme precipitation.

We start with the WCA between the extreme precipitation and the PDO when removing the effect of Niño 3.4. Figure 7 presents the results for the seven grids/cities (see Fig. S5 for all the 30 locations). A visual comparison of these results with wavelet coherence between PDO and extreme precipitation (Fig. 5) shows a significant reduction in the high power regions in the PWC (Fig. 7). Also, for most of the stations, there is no significant coherence between the extreme precipitation and PDO when the influence of Niño 3.4 is removed. For example, in the case of Gandhinagar and Jammu, a significant coherence between extreme precipitation and PDO at 8–16 and 16–32 years scale is observed when the influence of Niño 3.4 is yet included (Fig. 5), but it is missing without Niño 3.4 (Fig. 7). Similar observations are also made for the other stations (refer to Fig. S5). These reductions in the spatial areas of coherence imply that ENSO significantly contributes to the relationship between extreme precipitation and PDO. This is in accordance with the results reported by Wang et al. (2013), who showed that under the influence of ENSO, the variability of the PDO is slightly increased at the interannual timescale, but also shifts the PDO to a lower frequency at the decadal timescale. This also suggests that the variability of the Indian precipitation is forced by ENSO (Niño 3.4) via the influence of PDO, thus supporting the reports by Li et al. (2017) and Krishnamurthy and Krishnamurthy (2014).

Similarly, we consider the wavelet coherence between the extreme precipitation and IOD for the above seven locations after removal of Niño 3.4 (Fig. 8; see Fig. S6 for all 30 locations). Unlike the case with PDO, there are no significant changes in the wavelet coherence plots between the extreme precipitation and IOD before and after the removal of the effect of Niño 3.4. For example, comparing these two situations for Chennai (see Figs. 6, 8), no noticeable change in the significant coherence between the extreme precipitation and IOD is detected. This is also the case for the majority of the stations under investigation as well. These results imply that the Niño 3.4 and IOD operate at distinct modes and that the development and influence of IOD are independent of Niño 3.4. Similar observations were also made by, for example, Ashok et al. (2004) and Wang et al. (2017), who showed that the IOD and Niño 3.4 are independent factors influencing the Indian monsoon.

4.4 Reconstruction of oscillatory modes and spatial variability

To further understand the teleconnections of precipitation variability, modes at significant scales are extracted from the precipitation time series, and correlation with oscillations associated with Niño 3.4 and IOD is estimated (We do not present the results for PDO, since it is influenced by Niño 3.4). For this purpose, the wavelet coefficients are reconstructed at 2–4 years, 4–8 years, and 8–16 years bands.

The reconstructed bandpass component of the extreme precipitation and the climate indices are compared for all

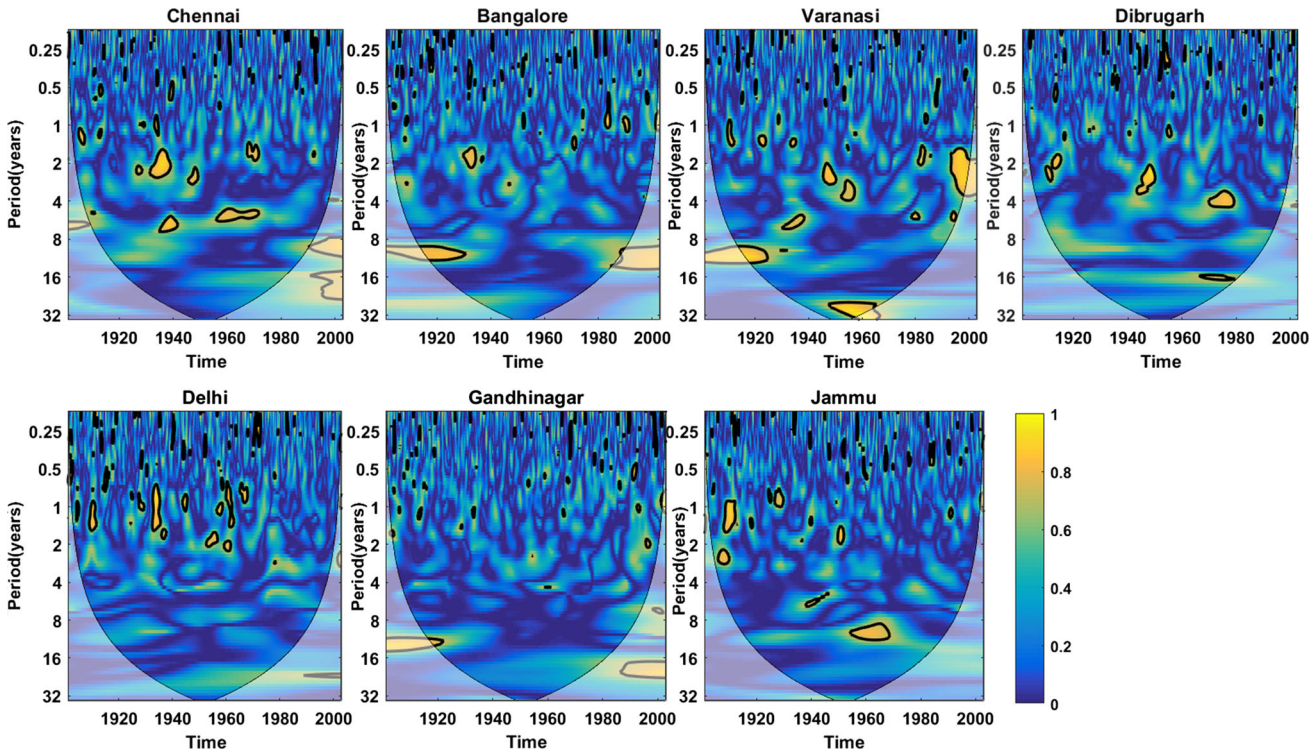

Fig. 7 Partial wavelet coherence spectra analysis between extreme precipitation from seven locations (one from each of the seven homogeneous regions) and PDO after removal of the influence of Niño 3.4 on precipitation. The black contour lines indicate the periods of statistically significant coherence with reference to red noise process

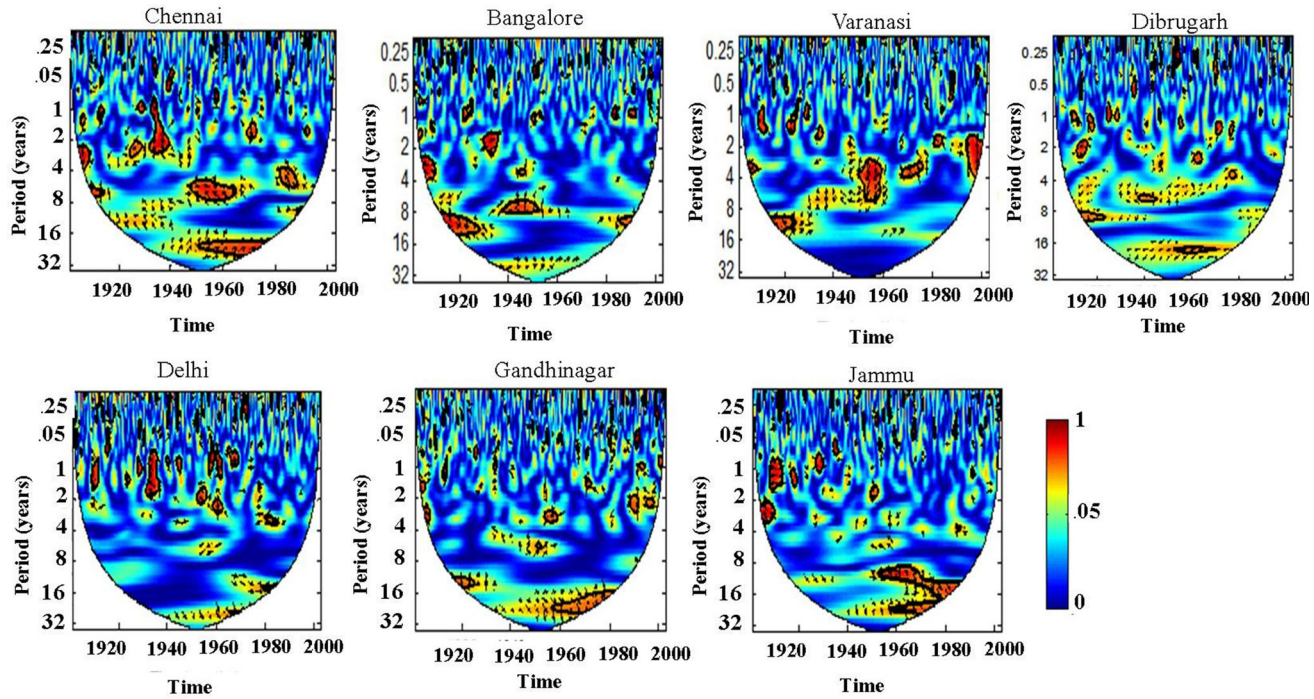

Fig. 8 Partial wavelet coherence spectra analysis between extreme precipitation from seven locations ((one from each of the seven homogeneous regions) and IOD after removal of the influence of Niño 3.4 on precipitation. The black contour lines indicate the periods of statistically significant coherence with reference to red noise process

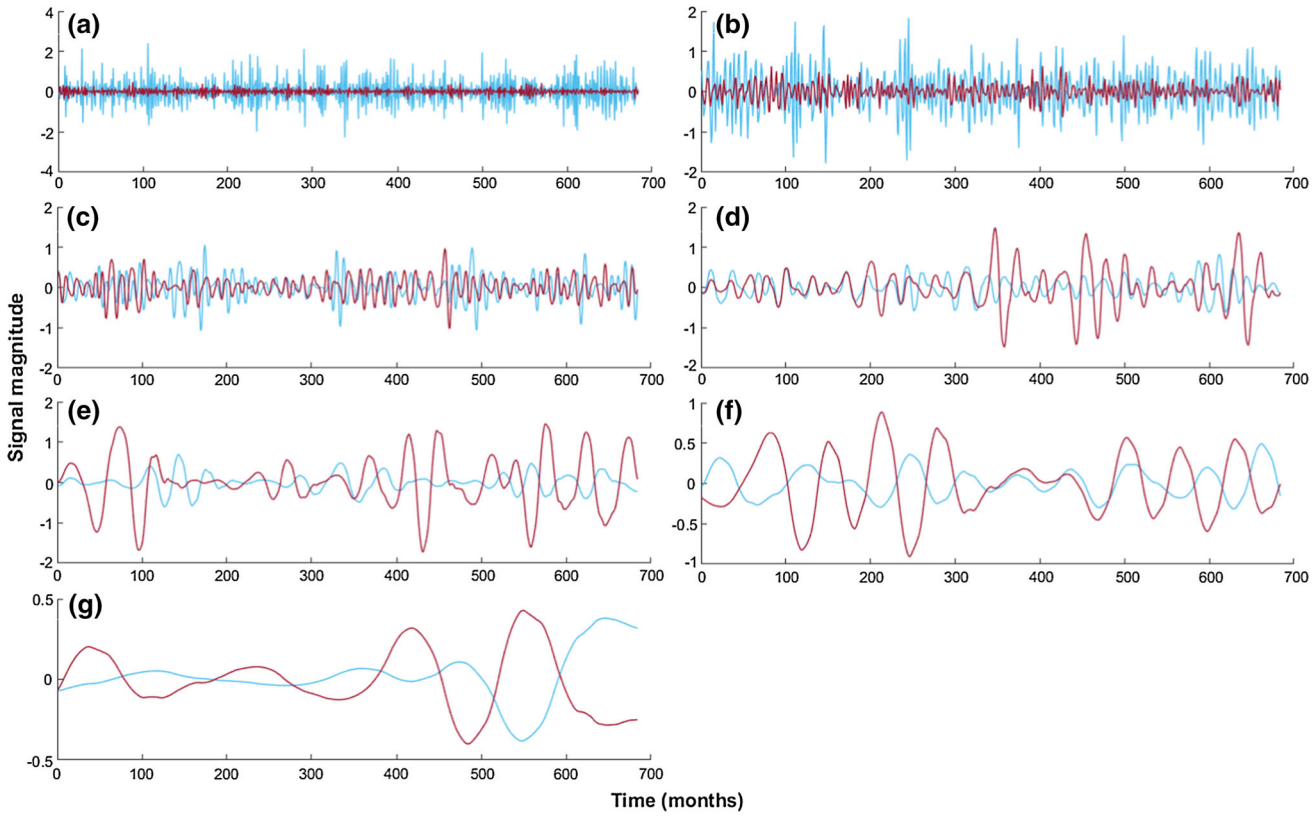

Fig. 9 Wavelet decomposition of Niño 3.4 (blue) and extreme precipitation (red) of one sample station (Chennai) at different temporal scales: **a** 2 months, **b** 4 months, **c** 8 months, **d** 16 months, **e** 32 months, **f** 64 months, **g** 128 months. The horizontal axis denotes the time in months and the vertical axis denotes the magnitude of the signal

the stations at seven different temporal scales: 2, 4, 8, 16, 32, 64, and 128 months. However, sample results are shown only for one station (Chennai, Figs. 9, 10). The results from the above analysis are presented for all the grid locations (Fig. 11) for the three indices in the form of a colour map of correlation coefficients at the three different scales considered above, i.e. 2–4 years (top), 4–8 years (middle), and 8–16 years (bottom). At all the scales, it is important to note that, the regions of significant correlation are similar for both Niño 3.4 and PDO, which reemphasize the results obtained from PWCA. It is also observed that the spatial correlation between the reconstructed modes of climate indices and precipitation at the different scales is nearly opposite. This might be possibly due to the negative and positive phase present in Niño 3.4, which gets captured at different timescales. Table 2 summarizes this in the form of percentage area having a significant positive or negative correlation with the climate indices. Here also, the results obtained from Niño 3.4 and PDO are very close, whereas distinct regions of significant correlation are obtained for Niño 3.4 and IOD.

The above results indicate that there is a generally negative association between precipitation modes and Niño 3.4 oscillations in almost all regions across India. However, the scale and nature of the association are spatially variable. For example, at 2–4 years scales, a negative correlation was observed between the two in the northern part during the period studied (1901–2013), whereas a positive correlation was observed in the southern part. Our results also reveal that a significant association existed only at long-term scales of the order of 8–16 years with IOD and at comparatively short-term scales of the order of 2–4 years and 4–8 years with Niño 3.4. The effect of Niño 3.4 and IOD was complementary to each other (Table 2). In the case of 2–4 years scale, the percentage area with positive (negative) Niño 3.4 influence was 17% (8%). However, the percentage area with negative (positive) IOD influence was 34% (6%). Finally, the results also reveal that the spatial variability of Niño 3.4 and PDO has almost the same patterns, which clearly strengthens the understanding that PDO's influence on Indian precipitation is not independent, rather it is through ENSO (Niño 3.4).

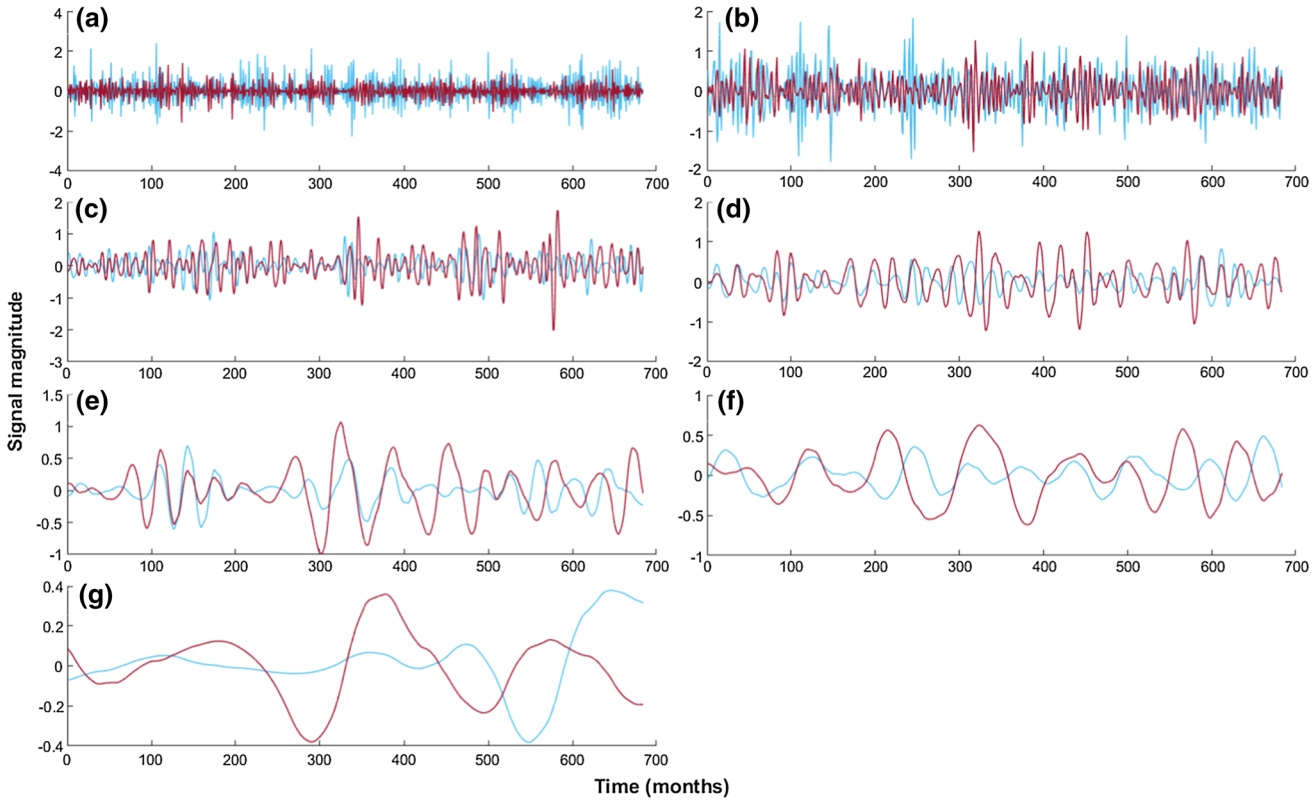

Fig. 10 Wavelet decomposition of IOD (blue) and extreme precipitation (red) of one sample station (Chennai) at different temporal scales: **a** 2 months, **b** 4 months, **c** 8 months, **d** 16 months, **e** 32 months, **f** 64 months, **g** 128 months. The horizontal axis denotes the time in months and the vertical axis denotes the magnitude of the signal

5 Discussion

The wavelet analysis of the extreme precipitation across 30 locations in India showed that dominant oscillations were found at 2–4 years, 8–16 years, and interdecadal scales. These oscillations were also found to vary with time and be short-lived. The wavelet coherence of the precipitation extremes with three prominent large-scale atmospheric circulation patterns, namely Niño 3.4, PDO, and IOD, revealed that Niño 3.4 had a significant coherence at 2–4 and 4–8 years scales, with most parts of the country showing that Niño 3.4 was responsible for the interannual variability in India. However, the influence of Niño 3.4 was not the same in all parts of the country. The precipitation in the eastern parts was significantly influenced by Niño 3.4, whereas the western and far north regions were not significantly affected by the Niño 3.4 oscillations. There were evidences of strong coherence at 8–16 years scale in the eastern parts of the country, which might be credited to the fact that interdecadal variations of Niño 3.4 teleconnections over the Indo-western Pacific is mainly governed by Niño 3.4 variance itself (Chowdary et al. 2012; Chowdhury and Beecham 2013).

Several studies (Kinter et al. 2002; Krishnamurthy and Krishnamurthy 2014) have proposed possible mechanisms linking the decadal change of the Niño 3.4-monsoon system to another large-scale climate variability. For example, Kinter et al. (2002) related this change to north Pacific SST and atmospheric circulation. Krishnamurthy and Krishnamurthy (2014) showed that the PDO could enhance (counteract) the Niño 3.4-monsoon relation when Niño 3.4 and PDO are in (out of) phase. The PWCA between the extreme precipitation and PDO after removing the effect of Niño 3.4 showed that the PDO did not have significant coherence between the precipitation events. This implies that PDO does not have direct influence over the decadal variability of precipitation, but rather that it has an indirect relation to enhancing the Niño 3.4-monsoon relationship, further supporting the observation made earlier by Krishnamurthy and Krishnamurthy (2014).

With reference to the relationship between the extreme precipitation and IOD, the wavelet coherence analysis showed that the IOD had a significant contribution to the precipitation variability at both interannual and decadal scales. Further, the PWCA analysis of precipitation and IOD after removing the effect of Niño 3.4 suggested that IOD events happened independently of Niño 3.4. This is in

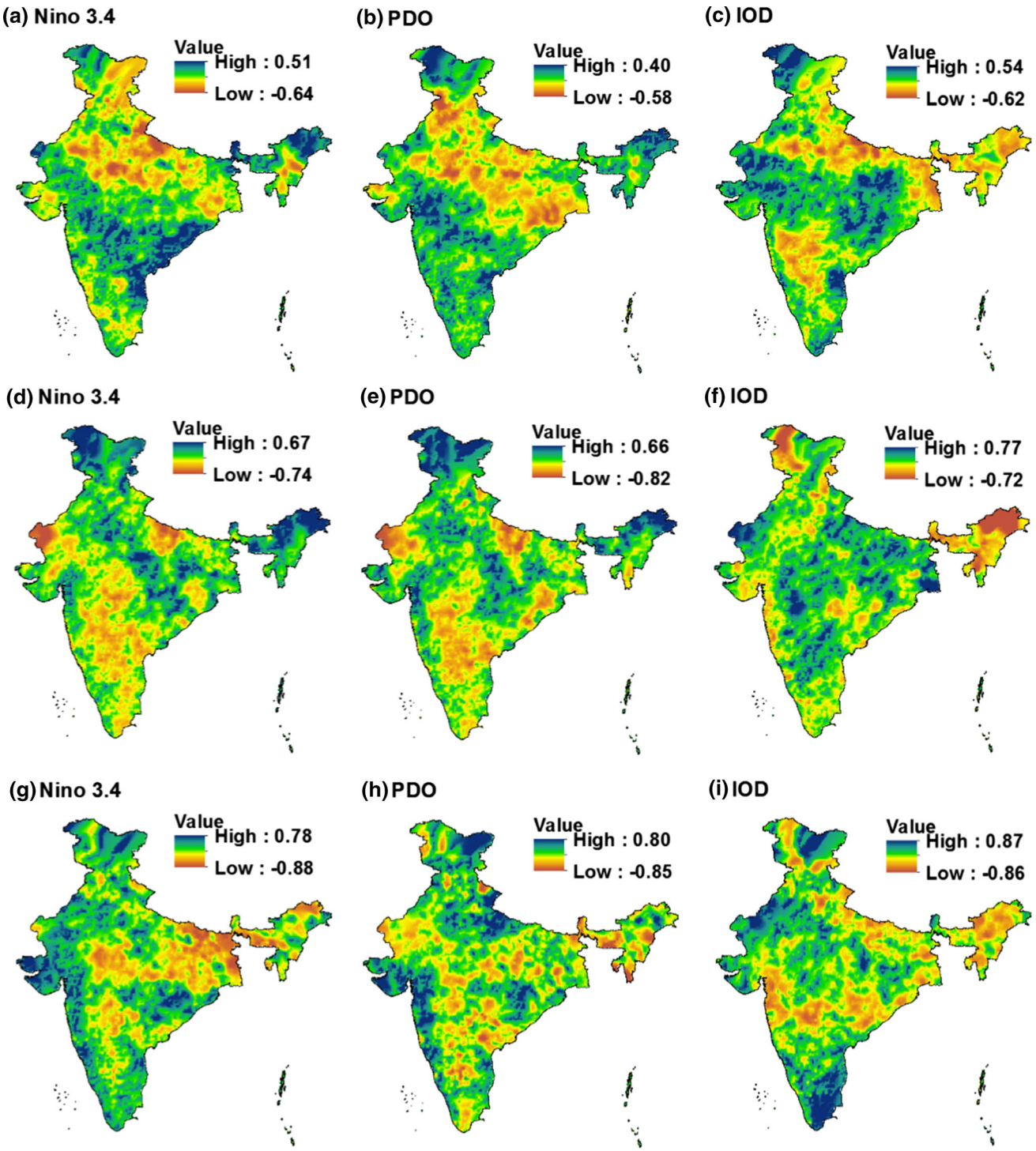

Fig. 11 Spatial variability of the correlation between the reconstructed modes of extreme precipitation and different climate indices at scales of 2–4 years (top), 4–8 years (middle) and 8–16 years (bottom)

line with the findings by some earlier studies (e.g. Ashok et al. 2004; Wang et al. 2016). For instance, Wang et al. (2016) showed that the climate model simulations without Niño 3.4 produced the most salient observed features of IOD even without Niño 3.4, including the relationships between the eastern and western poles at both the surface and the subsurface, as well as their seasonality. This suggests that Niño 3.4 is not fundamental to the existence of IOD. It is possible that the anomalies associated with IOD events are initiated through local wind response from the

Table 2 The percentage of total geographical area having significant positive or negative correlation with the climate indices

Climate indices	Negative	Zero	Positive
Niño3.4	8.38	74.35	17.27
PDO	25.44	67.33	7.23
IOD	34.07	59.36	6.56

Indian Ocean. This understanding is in agreement with the results reported by Ashok et al. (2004), who showed that the Indian Ocean Dipole Index is significantly coherent with the equatorial zonal winds in the central Indian Ocean. The coherence plots showed that coupling between extreme precipitation and Niño 3.4 had become stronger in the latter half of the time period studied (particularly after 1970). Cherchi and Navarra (2003) obtained similar results using a different approach and explained that this kind of behavior may be due to the changes occurred in the North Pacific after 1976 (Miller et al. 1994) and to the associated differences in the Niño 3.4 teleconnections (Deser and Blackmon 1995).

The results from the present study also revealed the existence of a complementary relationship of spatial variation of the association of precipitation with Niño 3.4 and IOD in most parts of India, except central India. However, in some parts of central India (including the eastern and western parts), the Niño 3.4 and IOD simultaneously influenced the precipitation but at different temporal scales. Further, it was observed that the coastal regions of peninsular, northeastern, and western regions were more significantly affected by Niño 3.4 and IOD in comparison with their counterparts in the inland region.

6 Conclusions

The wavelet analysis of the extreme data from gridded precipitation time series during 1901–2013 from different regions in the Indian sub-continent showed that the dominant oscillations varied both spatially and temporally. The present study examined, for the first time, the teleconnection between the interannual and interdecadal oscillations in extreme precipitation in India and three prominent atmospheric circulation patterns, namely Nino 3.4, PDO, and IOD. Wavelet analysis and its variants were employed. Important findings and conclusions are as follows:

1. The results from the application of the wavelet transform to extreme precipitation indicated that decadal and interdecadal oscillations (8–16 years and $>$ 16 years) were more significant than interannual (2–8 years) oscillations for the majority of the 30 stations studied. The oscillations varied both spatially and temporally at all the scales considered.
2. For all the seven homogeneous regions in India (identified by Agarwal et al. (2018)), the high-power wavelet coherence plots showed that the linkages between precipitation and the large-scale climate indices were time- and space-dependent. The partial wavelet coherence analysis also revealed two interesting findings:
   (a) There was a significant contribution of the Niño 3.4 to the relationship between extreme precipitation and the PDO. In other words, although PDO is a significantly important large-scale circulation pattern, it does not have direct linkage with the precipitation extremes in India. Rather, its influence is associated with its modulations with Niño 3.4 events.
   (b) Niño 3.4 and IOD were found to operate at distinct modes, and the development and influence of IOD were found to be independent of Niño 3.4. This observation is consistent with the results reported by earlier studies (e.g. Wang et al. 2016).

The results from the present study provided insights regarding the coupled behaviour of extreme precipitation in the Indian subcontinent with the changes in Niño 3.4 and IOD indices. The findings from this study can be useful for climate scientists to get a better understanding about the relationships between the extreme precipitation and atmospheric patterns. Further, this study also illustrated the importance of PWCA in such analysis.

Acknowledgements Maheswaran Rathinasamy acknowledges the funding support from the Inspire Faculty Award, Department of Science and Technology, India (IFA-12-ENG/28) and Science and Engineering Research Board (SERB), India (ECRA/16/1721). Ankit Agarwal was financially supported by Deutsche Forschungsgemeinschaft (DFG) (GRK 2043/1) within the graduate research training group Natural risk in a changing world (NatRiskChange) at the University of Potsdam (http://www.uni-potsdam.de/natriskchange).

References

Addison PS (2005) Wavelet transforms and the ECG: a review. Physiol Meas 26(5):R155–R199. https://doi.org/10.1088/0967-3334/26/5/R01

Agarwal A (2019) Unraveling spatio-temporal climatic patterns via multi-scale complex networks. Universität Potsdam, Potsdam

Agarwal A, Maheswaran R, Kurths J, Khosa R (2016) Wavelet spectrum and self-organizing maps-based approach for hydrologic regionalization—a case study in the Western United States. Water Resour Manag 30(12):4399–4413. https://doi.org/10.1007/s11269-016-1428-1

Agarwal A, Marwan N, Maheswaran R, Merz B, Kurths J (2018) Quantifying the roles of single stations within homogeneous regions using complex network analysis. J Hydrol. https://doi.org/10.1016/j.jhydrol.2018.06.050

Agarwal A, Caesar L, Marwan N, Maheswaran R, Merz B, Kurths J (2019) Network-based identification and characterization of teleconnections on different scales. Sci Rep. https://doi.org/10.1038/s41598-019-45423-5

Alexander LV, Uotila P, Nicholls N (2009) Influence of sea surface temperature variability on global temperature and precipitation extremes. J Geophys Res. https://doi.org/10.1029/2009jd012301

Araghi A, Mousavi-Baygi M, Adamowski J, Martinez C (2017) Association between three prominent climatic teleconnections and precipitation in Iran using wavelet coherence. Int J Climatol 37(6):2809–2830. https://doi.org/10.1002/joc.4881

Ashok K, Guan Z, Saji NH, Yamagata T (2004) Individual and combined influences of ENSO and the Indian Ocean Dipole on the Indian Summer Monsoon. J Clim 17(16):3141–3155. https://doi.org/10.1175/1520-0442(2004)017%3c3141:IACIOE%3e2.0.CO;2

Ashok K, Behera SK, Rao SA, Weng H, Yamagata T (2007) El Niño Modoki and its possible teleconnection. J Geophys Res. https://doi.org/10.1029/2006jc003798

Azad S, Rajeevan M (2016) Possible shift in the ENSO-Indian monsoon rainfall relationship under future global warming. Sci Rep. https://doi.org/10.1038/srep20145

Behera SK, Ratnam JV (2018) Quasi-asymmetric response of the Indian summer monsoon rainfall to opposite phases of the IOD. Sci Rep. https://doi.org/10.1038/s41598-017-18396-6

Bhatla R, Singh AK, Mandal B, Ghosh S, Pandey SN, Sarkar A (2016) Influence of North Atlantic oscillation on Indian summer monsoon rainfall in relation to quasi-binneal oscillation. Pure Appl Geophys 173(8):2959–2970. https://doi.org/10.1007/s00024-016-1306-z

Boers N, Goswami B, Rheinwalt A, Bookhagen B, Hoskins B, Kurths J (2019) Complex networks reveal global pattern of extreme-rainfall teleconnections. Nature. 566:373–377. https://doi.org/10.1038/s41586-018-0872-x

Cazes-Boezio G, Robertson AW, Mechoso CR (2003) Seasonal dependence of ENSO teleconnections over South America and relationships with precipitation in Uruguay. J Clim 16(8):1159–1176. https://doi.org/10.1175/1520-0442(2003)16%3c1159:SDOETO%3e2.0.CO;2

Cherchi A, Navarra A (2003) Reproducibility and predictability of the Asian summer monsoon in the ECHAM4-GCM. Clim Dyn 20(4):365–379. https://doi.org/10.1007/s00382-002-0280-6

Chowdary JS, Xie S-P, Tokinaga H, Okumura YM, Kubota H, Johnson N, Zheng X-T (2012) Interdecadal variations in ENSO teleconnection to the indo-Western Pacific for 1870–2007*. J Clim 25(5):1722–1744. https://doi.org/10.1175/JCLI-D-11-00070.1

Chowdhury RK, Beecham S (2013) Influence of SOI, DMI and Niño3.4 on South Australian rainfall. Stoch Environ Res Risk Assess 27(8):1909–1920. https://doi.org/10.1007/s00477-013-0726-x

Cioffi F, Conticello F, Lall U, Marotta L, Telesca V (2017) Large scale climate and rainfall seasonality in a Mediterranean Area: insights from a non-homogeneous Markov model applied to the Agro-Pontino plain: climate seasonality in Agro Pontino Plain. Hydrol Process 31(3):668–686. https://doi.org/10.1002/hyp.11061

Curtis S, Salahuddin A, Adler RF, Huffman GJ, Gu G, Hong Y (2007) Precipitation extremes estimated by GPCP and TRMM: eNSO relationships. J Hydrometeorol 8(4):678–689. https://doi.org/10.1175/JHM601.1

Daubechies I (1992) Ten lectures on wavelets. Society for Industrial and Applied Mathematics, New York

Deser C, Blackmon ML (1995) On the relationship between tropical and North Pacific sea surface temperature variations. J Clim 8(6):1677–1680. https://doi.org/10.1175/1520-0442(1995)008%3c1677:OTRBTA%3e2.0.CO;2

Duan W, He B, Takara K, Luo P, Hu M, Alias NE, Nover D (2015) Changes of precipitation amounts and extremes over Japan between 1901 and 2012 and their connection to climate indices. Clim Dyn 45(7–8):2273–2292. https://doi.org/10.1007/s00382-015-2778-8

Ekhtiari N, Agarwal A, Marwan N, Donner RV (2019) Disentangling the multi-scale effects of sea-surface temperatures on global precipitation: a coupled networks approach. Chaos Interdiscip J Nonlinear Sci 29(6):063116. https://doi.org/10.1063/1.5095565

Flandrin P (1988) A time–frequency formulation of optimum detection. IEEE Trans Acoust Speech Signal Process 36(9):1377–1384. https://doi.org/10.1109/29.90365

Foufoula-Georgiou E, Kumar P (eds) (1994) Wavelets in geophysics. Academic Press, San Diego

Gan TY, Gobena AK, Wang Q (2007) Precipitation of southwestern Canada: wavelet, scaling, multifractal analysis, and teleconnection to climate anomalies: Precipitation Variability of SW Canada. J Geophys Res Atmos. https://doi.org/10.1029/2006jd007157

Grimm AM (2011) Interannual climate variability in South America: impacts on seasonal precipitation, extreme events, and possible effects of climate change. Stoch Environ Res Risk Assess 25(4):537–554. https://doi.org/10.1007/s00477-010-0420-1

Grimm AM, Tedeschi RG (2009) ENSO and extreme rainfall events in South America. J Clim 22(7):1589–1609. https://doi.org/10.1175/2008JCLI2429.1

Grinsted A, Moore JC, Jevrejeva S (2004) Application of the cross wavelet transform and wavelet coherence to geophysical time series. Nonlinear Process Geophys 11(5/6):561–566. https://doi.org/10.5194/npg-11-561-2004

Hanley DE, Bourassa MA, O'Brien JJ, Smith SR, Spade ER (2003) A quantitative evaluation of ENSO indices. J Clim 16(8):1249–1258. https://doi.org/10.1175/1520-0442(2003)16%3c1249:AQEOEI%3e2.0.CO;2

Ihara C, Kushnir Y, Cane MA (2008) Warming trend of the Indian ocean SST and Indian ocean dipole from 1880 to 2004*. J Clim 21(10):2035–2046. https://doi.org/10.1175/2007JCLI1945.1

Khedun CP, Mishra AK, Singh VP, Giardino JR (2014) A copula-based precipitation forecasting model: investigating the inter-decadal modulation of ENSO's impacts on monthly precipitation: Copula-Based Precipitation Forecasting Models. Water Resour Res 50(1):580–600. https://doi.org/10.1002/2013WR013763

Kim T-W, Yoo C, Ahn J-H (2008) Influence of climate variation on seasonal precipitation in the Colorado River Basin. Stoch Environ Res Risk Assess 22(3):411–420. https://doi.org/10.1007/s00477-007-0126-1

Kinter JL, Miyakoda K, Yang S (2002) Recent change in the connection from the Asian monsoon to ENSO. J Clim 15(10):1203–1215. https://doi.org/10.1175/1520-0442(2002)015%3c1203:RCITCF%3e2.0.CO;2

Konapala G, Valiya Veettil A, Mishra AK (2018) Teleconnection between low flows and large-scale climate indices in Texas River basins. Stoch Environ Res Risk Assess 32(8):2337–2350. https://doi.org/10.1007/s00477-017-1460-6

Krishnamurthy V, Goswami BN (2000) Indian monsoon–ENSO relationship on interdecadal timescale. J Clim 13(3):579–595. https://doi.org/10.1175/1520-0442(2000)013%3c0579:IMEROI%3e2.0.CO;2

Krishnamurthy L, Krishnamurthy V (2014) Influence of PDO on South Asian summer monsoon and monsoon–ENSO relation. Clim Dyn 42(9–10):2397–2410. https://doi.org/10.1007/s00382-013-1856-z

Krishnamurthy L, Krishnamurthy V (2016) Teleconnections of Indian monsoon rainfall with AMO and Atlantic tripole. Clim Dyn 46(7–8):2269–2285. https://doi.org/10.1007/s00382-015-2701-3

Krishnan R, Sugi M (2003) Pacific decadal oscillation and variability of the Indian summer monsoon rainfall. Clim Dyn 21(3–4):233–242. https://doi.org/10.1007/s00382-003-0330-8

Kumar KK (1999) On the weakening relationship between the Indian Monsoon and ENSO. Science 284(5423):2156–2159. https://doi.org/10.1126/science.284.5423.2156

Kurths J, Agarwal A, Shukla R, Marwan N, Rathinasamy M, Caesar L, Krishnan R, Merz B (2019) Unravelling the spatial diversity of Indian precipitation teleconnections via a non-linear multi-scale approach. Nonlinear Process Geophys 26(3):251–266. https://doi.org/10.5194/npg-26-251-2019

Lakhanpal A, Sehgal V, Maheswaran R, Khosa R, Sridhar V (2017) A non-linear and non-stationary perspective for downscaling mean monthly temperature: a wavelet coupled second order Volterra model. Stoch Environ Res Risk Assess 31(9):2159–2181. https://doi.org/10.1007/s00477-017-1444-6

Li Q, Chen J (2014) Teleconnection between ENSO and climate in South China. Stoch Environ Res Risk Assess 28(4):927–941. https://doi.org/10.1007/s00477-013-0793-z

Li G, Chen J, Wang X, Tan Y, Jiang X (2017) Modulation of Pacific Decadal Oscillation on the relationship of El Niño with southern China rainfall during early boreal winter. Atmos Res Lett 18(8):336–341

Lorenzo MN, Taboada JJ, Gimeno L (2008) Links between circulation weather types and teleconnection patterns and their influence on precipitation patterns in Galicia (NW Spain). Int J Climatol 28(11):1493–1505. https://doi.org/10.1002/joc.1646

Maity R, Nagesh Kumar D (2006) Bayesian dynamic modeling for monthly Indian summer monsoon rainfall using El Niño-Southern Oscillation (ENSO) and Equatorial Indian Ocean Oscillation (EQUINOO). J Geophys Res. https://doi.org/10.1029/2005jd006539

Maraun D, Kurths J (2004) Cross wavelet analysis: significance testing and pitfalls. Nonlinear Process Geophys 11(4):505–514. https://doi.org/10.5194/npg-11-505-2004

Mihanović H, Orlić M, Pasarić Z (2009) Diurnal thermocline oscillations driven by tidal flow around an island in the Middle Adriatic. J Mar Syst 78:S157–S168. https://doi.org/10.1016/j.jmarsys.2009.01.021

Miller JR, Russell GL, Caliri G (1994) Continental-scale river flow in climate models. J Clim 7(6):914–928. https://doi.org/10.1175/1520-0442(1994)007%3c0914:CSRFIC%3e2.0.CO;2

Mokhov II, Smirnov DA, Nakonechny PI, Kozlenko SS, Kurths J (2012) Relationship between El-Niño/Southern oscillation and the Indian monsoon. Izv Atmos Ocean Phys 48(1):47–56. https://doi.org/10.1134/S0001433812010082

Ng EKW, Chan JCL (2012) Interannual variations of tropical cyclone activity over the north Indian Ocean. Int J Climatol 32(6):819–830. https://doi.org/10.1002/joc.2304

Niu J (2013) Precipitation in the Pearl River basin, South China: scaling, regional patterns, and influence of large-scale climate anomalies. Stoch Environ Res Risk Assess 27(5):1253–1268. https://doi.org/10.1007/s00477-012-0661-2

Niu J, Chen J, Sivakumar B (2014) Teleconnection analysis of runoff and soil moisture over the Pearl River basin in southern China. Hydrol Earth Syst Sci 18(4):1475–1492. https://doi.org/10.5194/hess-18-1475-2014

Pai DS, Sridhar L, Badwaik MR, Rajeevan M (2015) Analysis of the daily rainfall events over India using a new long period (1901–2010) high resolution (0.25° × 0.25°) gridded rainfall data set. Clim Dyn 45(3–4):755–776. https://doi.org/10.1007/s00382-014-2307-1

Rheinwalt A, Goswami B, Boers N, Heitzig J, Marwan N, Krishnan R, Kurths J (2015) Teleconnections in climate networks: a network-of-networks approach to investigate the influence of sea surface temperature variability on monsoon systems. In: Lakshmanan V, Gilleland E, McGovern A, Tingley M (eds) Machine learning and data mining approaches to climate science. Springer, Cham, pp 23–33

Shi H, Li T, Wei J, Fu W, Wang G (2016) Spatial and temporal characteristics of precipitation over the three-river headwaters region during 1961–2014. J Hydrol Reg Stud 6:52–65. https://doi.org/10.1016/j.ejrh.2016.03.001

Tan X, Gan TY, Shao D (2016) Wavelet analysis of precipitation extremes over Canadian ecoregions and teleconnections to large-scale climate anomalies: large precipitation and climate anomalies. J Geophys Res Atmos 121(24):14469–14486. https://doi.org/10.1002/2016JD025533

Torrence C, Compo GP (1998) A practical guide to wavelet analysis. Bull Am Meteorol Soc 79(1):61–78. https://doi.org/10.1175/1520-0477(1998)079%3c0061:APGTWA%3e2.0.CO;2

Wang B, Liu J, Kim H-J, Webster PJ, Yim S-Y, Xiang B (2013) Northern Hemisphere summer monsoon intensified by mega-El Nino/southern oscillation and Atlantic multidecadal oscillation. Proc Natl Acad Sci 110(14):5347–5352. https://doi.org/10.1073/pnas.1219405110

Wang H, Chen Y, Li W (2014) Hydrological extreme variability in the headwater of Tarim River: links with atmospheric teleconnection and regional climate. Stoch Environ Res Risk Assess 28(2):443–453. https://doi.org/10.1007/s00477-013-0763-5

Wang H, Kumar A, Murtuguddhe R (2016) Interaction between the indian ocean dipole and ENSO associated with ocean subsurface variability, science and technology infusion climate bulletin. In: 41st NOAA annual climate diagnostics and prediction workshop, Orono, 3–6 October

Wang C, Deser C, Yu J-Y, DiNezio P, Clement A (2017) El Niño and southern oscillation (ENSO): A Review. In: Glynn PW, Manzello DP, Enochs IC (eds) Coral reefs of the eastern tropical pacific, vol 8. Springer, Dordrecht, pp 85–106

Yoon S-K, Kim J-S, Lee J-H, Moon Y-I (2013) Hydrometeorological variability in the Korean Han River Basin and its sub-watersheds during different El Niño phases. Stoch Environ Res Risk Assess 27(6):1465–1477. https://doi.org/10.1007/s00477-012-0683-9

Zhao Y, Zou X, Cao L, Xu X (2014) Changes in precipitation extremes over the Pearl River Basin, southern China, during 1960–2012. Quat Int 333:26–39. https://doi.org/10.1016/j.quaint.2014.03.060